Orthotropic electro-thermal behaviour of highly-aligned carbon nanotube web based composites

Composites Science and Technology 170 (2019) 157–164

Contents lists available at ScienceDirect

Composites Science and Technology

journal homepage: www.elsevier.com/locate/compscitech

Orthotropic electro-thermal behaviour of highly-aligned carbon nanotube web based composites

Xudan Yao[a], Brian G. Falzon[a,*], Stephen C. Hawkins[a,b]

[a] Advanced Composites Research Group, School of Mechanical and Aerospace Engineering, Queen's University Belfast, BT9 5AH, UK
[b] Dept. of Materials Science and Engineering, Monash University, Clayton, Vic., 3800, Australia

ARTICLE INFO

Keywords:
Carbon nanotube web
Composite
Electro-thermal behaviour
Orthotropic
Orientation
Layup

ABSTRACT

A 'forest' of vertically aligned carbon nanotubes (CNTs), synthesised by chemical vapour deposition with an iron catalyst on a silicon substrate, is drawn into a horizontally-aligned CNT web. Previous work has shown that the electro-thermal properties of this web may be tuned by altering the individual length of the CNTs and the number of layers. This paper demonstrates, for the first time, that the orientation and multi-directional layering of the web provides further scope for tuning the electrical conductivity and heat distribution of the composite system. An analytical model based on the thermal conduction theory of anisotropic solids is proposed to predict the electrical conductivity of general multi-layered and multi-directional CNT webs.

Specimens with different aspect ratios and web orientations were manufactured and their electrical conductivity and resistive heat distribution measured. All of them were shown to exhibit electrical properties and heating distributions which could be predicted or bounded by the analytical model. Consequently, through tuning the CNT web orientation and layup, various heating patterns may be obtained and designed for specific requirements.

1. Introduction

Carbon fibre reinforced polymer (CFRP) composite is the predominant material used for the primary structure of the latest generation of wide-body passenger aircraft (e.g. 53 wt% on the Airbus A350 XWB and 50 wt% on the Boeing 787 [1]) delivering a 20% weight reduction over comparable previous-generation aircraft and commensurate reductions in fuel consumption. With an incessant drive towards greater efficiency, the industry is seeking novel solutions to reducing energy and maintenance requirements of on-board systems. One such system is the conventional ice protection system used on most aircraft for anti-icing. This relies on hot air bleed ducted from the engine compressor stages, adding non-structural weight and maintenance complexity. More recently, electro-conductive textiles [2] and metallic wires [3] have been proposed as the heating element of electrically-powered systems. Indeed, while the A350 utilises a conventional ice-protection system, the B787 makes use of an electrical system for wing anti-icing, developed by GKN, where the heating element is a metal spray applied between two insulating glass fibre plies [4]. Interestingly, the anti-icing system used on the nacelles of the B787 remains a conventional engine bleed system.

Owing to their negligible weight, high electrical and thermal conductivity, and compatibility with CFRP, carbon nanomaterials, including carbon nanotubes (CNTs) and graphene [5–9], have been proposed as promising heating elements for anti-icing/de-icing (AI/DI) electro-thermal systems. However, both randomised CNTs [6,10–12] and graphene [7–9,13,14] need to be uniformly dispersed before being applied as the heating element. Aligned assemblies such as 'fuzzy fibres' (CNTs grown directly onto CF) [15,16], continuous aerogel-formed CNT films [17–19], directly drawn CNT webs [5,20] and 'sheared' forests of CNTs [21–23] have also been investigated as has the influence of CNT volume fraction, on electrical [24] and thermal [25] conductivities.

Compared with other aligned assemblies, directly drawn CNT web, produced by drawing a continuous sheet of CNTs from specially grown CNT forests [26], is essentially catalyst and defect free, is of negligible weight and highly tuneable. The CNT web is orthotropic, with the CNTs being highly aligned and conductive along the draw direction. The CNT web has been widely studied to fabricate transparent film heaters [27–31]. Moreover, we have demonstrated the use of this material as a promising heating element for AI/DI applications [5,20]. However, previous research only utilised unidirectional CNT webs in the draw direction, without considering the influence of different orientations, and layups.

* Corresponding author.
E-mail address: b.falzon@qub.ac.uk (B.G. Falzon).

https://doi.org/10.1016/j.compscitech.2018.11.042
Received 19 February 2018; Received in revised form 19 August 2018; Accepted 25 November 2018
Available online 04 December 2018

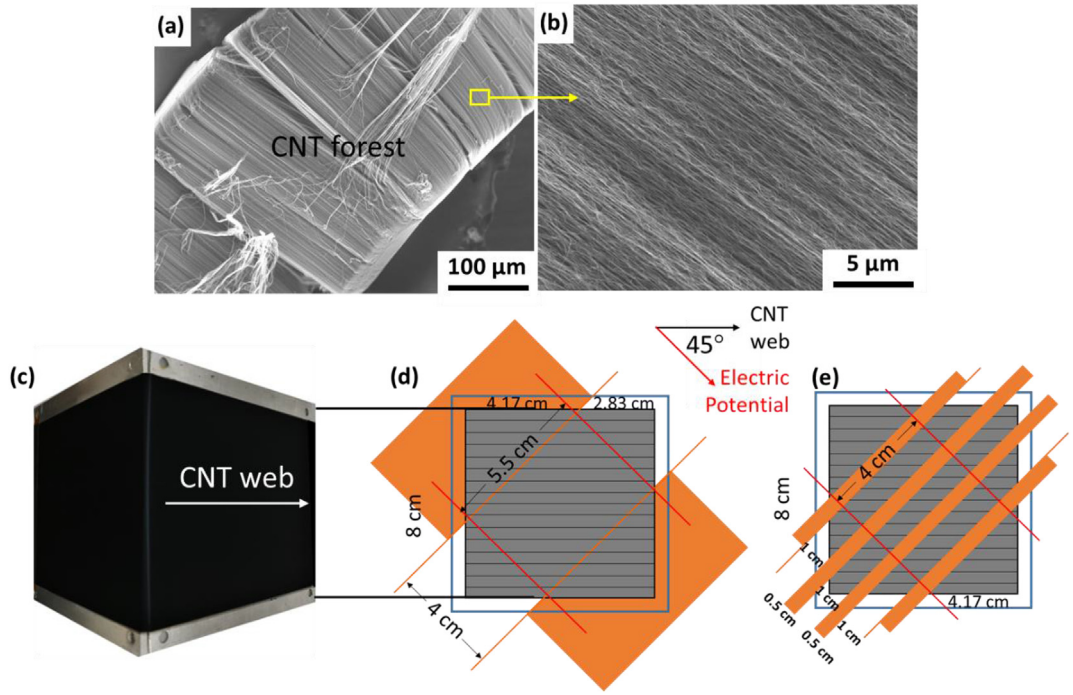

Fig. 1. (a, b) SEM images of a vertically-aligned CNT forest, (c) directly drawn CNT webs on aluminium frames; (d) sample preparation, with a single CNT web orientation of 45° to the electric potential, of a low aspect ratio (40 mm × 55 mm) and (e) higher aspect ratio (10 mm × 40 mm).

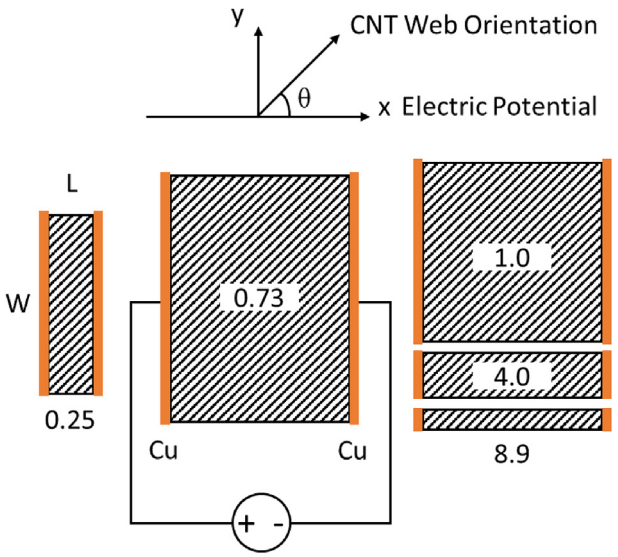

Fig. 2. CNT web composite with different aspect ratios (L/W = 0.25, 0.73, 1.0, 4.0, 8.9) subject to the electric potential at an angle θ to the CNT web orientation.

Altering the length of individual CNTs, and the number of web layers, provides a measure of control over the resulting thermal and electrical transport characteristics of the system. In this work, further tailoring of electro-thermal properties is achieved by the novel approach of exploiting the effect of the orientation and layup of the CNT webs, which exhibit orthotropic conductivity. An analytical model is presented which can be used to not only predict the effective conductivity properties of a multidirectional 'web laminate', but also help to design an ice protection system to meet specific requirements.

2. Materials and methods

2.1. Materials

Vertically aligned CNT forests (Fig. 1a and b) were synthesised by chemical vapour deposition (CVD) of acetylene, at a temperature of 700 °C, on silicon wafer with iron as the catalyst, yielding an average CNT length of 300 μm and an average diameter of 10 nm [20,32]. The CNT web is obtained by directly drawing a continuous sheet of horizontally oriented CNTs from the forests and winding onto four mounted aluminium frames (Fig. 1c) to the requisite number of layers. The web is transferred from a frame and embedded between two layers of glass fibre (GF) prepreg (Gurit RE295/SE84LV GF/epoxy woven prepreg with an areal density of 600 g m^{-2}), where the prepreg works as the support as well as the insulator. Copper foil strips (Alfa Aeser, 25 μm thick) were used as the electrical buses connecting the web (Fig. 1d and e).

2.2. Sample preparation and characterization

In order to investigate the effect of CNT web orientation, layup and sample geometry, on the electro-thermal properties, two sets of samples were prepared. For the 1st set, test coupons with different aspect ratios (L/W of 0.25, 0.73, 1.0, 4.0 and 8.9 which respectively correspond to specimens with an effective CNT web area of 10 mm × 40 mm, 40 mm × 55 mm, 40 mm × 40 mm, 40 mm × 10 mm and 40 mm × 4.5 mm) and CNT web orientations (θ = 0°, 10°, 22.5°, 45°, 67.5°, 90°, where θ is the angle between the CNT web alignment and the electric potential) were prepared (Fig. 2, Table 1). Note that 'L' refers to the web length (i.e. distance between the copper buses) while 'W' refers to the width of web in contact with each bus (Fig. 2). The 2nd set were all either 40 mm × 40 mm (i.e. L/W = 1) or 40 mm × 10 mm (L/W = 4) and comprised composites with different CNT web layup: [0_4], [45_4], [90_4], [0_2/22.5_2], [0_2/45_2], [0_2/90_2], [$+22.5_2$/-22.5_2], [$+45_2$/-45_2], [$+67.5_2$/-67.5_2], [22.5_2/-67.5_2] and [0/+45/-45/90] (Table 2).

As previously reported [20,33], 20 layers of CNT web (0.38 g m^{-2})

Table 1
1st set of samples with various CNT web orientation and aspect ratio.

θ (°)	Dimension (mm x mm)	10 × 40	40 × 55	40 × 40	40 × 10	40 × 4.5
	Aspect Ratio (L/W)	0.25	0.73	1.0	4.0	8.9
0	Number of Specimens	3	1	1	3	3
10		3	1	0	3	3
22.5		3	1	0	3	3
45		3	1	1	3	3
67.5		3	1	0	3	3
90		3	1	1	3	3

Table 2
2nd set of samples with different CNT web layup.

Sample designation	Layup of CNT webs[a]	Dimension (mm x mm)	40 × 40	40 × 10
		Aspect Ratio (L/W)	1.0	4.0
1	$[0_4]$	Number of Specimens	1	3
2	$[45_4]$		1	3
3	$[90_4]$		1	3
4	$[0_2/22.5_2]$		1	3
5	$[0_2/45_2]$		1	3
6	$[0_2/90_2]$		1	3
7	$[+22.5_2/-22.5_2]$		1	3
8	$[+45_2/-45_2]$		1	3
9	$[+67.5_2/-67.5_2]$		1	3
10	$[22.5_2/-67.5_2]$		1	3
11	[0/+45/-45/90]		1	3

[a] Note: 5 layers of CNT web was treated as a unit, i.e. $[0_4]$ represents 20 layers.

have suitable electrical resistance and reproducibility for the specimen dimensions being used, thus 20 CNT layers were used for all of the samples in this study. When the CNT webs were prepared and embedded in the GF prepreg, with the designated orientation and layup, the whole assembly was vacuum-bagged and cured at 120 °C for 1 hour. The composite samples were subsequently cut to the desired aspect ratio with a Struers Accutom-50 cutting machine.

The morphology of CNTs was observed using a JSM-6500F Field Emission Scanning Electron Microscope (Fig. 1a and b). The resistance of the samples was measured by an Agilent 34450A 5½ Digit Multimeter, utilizing the 4-wire method. An EA Elektro-Automatik PS 3016-20B Digital Bench Power Supply was employed to supply the constant voltage, and the heat distribution of the samples was monitored by an FLIR SC640 thermal imaging (IR) camera.

3. Results and discussion

3.1. Effect of CNT web orientation and sample aspect ratio

3.1.1. Effect on electrical conductivity

The conductivities of specimens with different aspect ratios (L/W = 0.25, 0.73, 1.0, 4.0, 8.9) and web orientations (θ = 0°, 10°, 22.5°, 45°, 67.5°, 90°) were measured and compared to analytical predictions (Fig. 3) based on the thermal conductivity theory of anisotropic solids [34–36]. That work used the expressions 'finite' and 'infinite' to denote extremum dimensions of the samples, in terms of aspect ratio. Our samples are, likewise, defined in terms of their aspect ratio which can vary from L > > W (i.e. tending to infinity, or where the distance between the copper buses is much greater than their contact with the web) to L < < W (i.e. tending to zero, or where the contact is much greater than the distance between the buses).

The thickness of 20 layers of CNT web in resin is ~12 μm, which

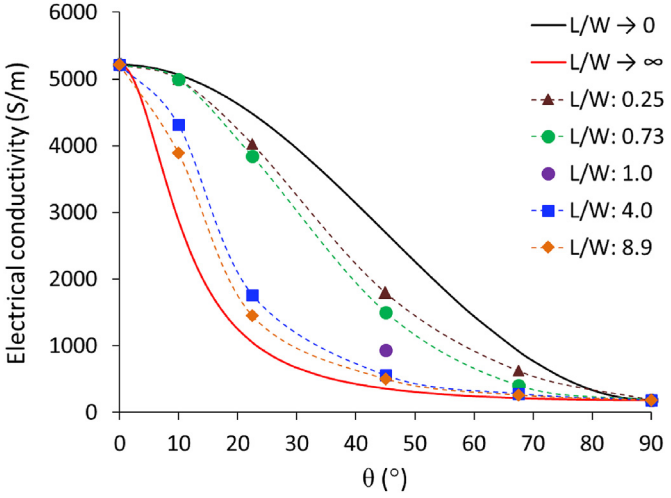

Fig. 3. Electrical conductivity of the CNT web composite at five different aspect ratios (L/W) with various CNT web orientations (θ from 0° to 90°).

can be neglected compared with the length and width of the specimens, thus the laminate can be treated as a two-dimensional system. As the CNT web is highly aligned and conductive in the draw direction, with low conductivity in the transverse direction [20], the composite systems are orthotropic. As a consequence, two situations should be discussed based on the CNT web orientation [37]; when the CNT webs are parallel or perpendicular to the applied electric field gradient, the conductivity will be the longitudinal (σ_l) or transverse (σ_t) conductivity, respectively, and is not affected by the sample geometry (i.e. aspect ratio). Otherwise, the aspect ratio can have a significant effect. When the sample aspect ratio tends to zero (L/W→0), the conductivity tensor [32,33] is given by Equations (1)–(3),

$$[\hat{\sigma}] = \begin{bmatrix} \sigma_l \cos^2\theta + \sigma_t sin^2\theta & \frac{\sigma_l - \sigma_t}{2}\sin 2\theta \\ \frac{\sigma_l - \sigma_t}{2}\sin 2\theta & \sigma_l \sin^2\theta + \sigma_t \cos^2\theta \end{bmatrix} \quad (1)$$

$$\begin{bmatrix} J_x \\ J_y \end{bmatrix} = \begin{bmatrix} \sigma_x & \sigma_{xy} \\ \sigma_{xy} & \sigma_y \end{bmatrix} \cdot \begin{bmatrix} E_x \\ E_y \end{bmatrix} \quad (2)$$

$$\sigma_x = \sigma_l \cos^2\theta + \sigma_t sin^2\theta \quad (3)$$

where J represents the current density and E represents the electric field.

When the sample aspect ratio tends to infinity (L/W→∞), the relatively long free web edges will affect the current flow and modify the axial conductivity compared with the L < < W samples [34,35]:

$$\sigma_x = (\sigma_l \cos^2\theta + \sigma_t sin^2\theta) - \frac{(\sigma_l - \sigma_t)^2 \sin^2\cos^2\theta}{\sigma_l \sin^2\theta + \sigma_t \cos^2\theta} \quad (4)$$

Both L/W→0 and L/W→∞ curves based on equations (3) and (4) are shown in Fig. 3, together with the experimental results of the 1st set of specimens. The electrical conductivity of CNT web composites of any dimension shows the expected relationship with angle (θ, Fig. 2). When the aspect ratio decreases, the conductivity curve tends towards the L/W→0 curve (asymptote), whereas when the aspect ratio increases, it approaches the L/W→∞ curve. As a consequence, depending on the aspect ratio of the specimens (Fig. 3), the conductivity, as a function of web orientation, is bounded by the two theoretical curves for zero and infinite aspect ratios. This is consistent with results obtained for thermal conductivities of carbon fibre reinforced composites [35].

3.1.2. Effect on heating performance

Samples with L/W of 0.73 and 4.0 were tested at a constant voltage of 12 V and 16 V respectively in order to understand the effect of the CNT web orientation and sample geometry on the heating performance.

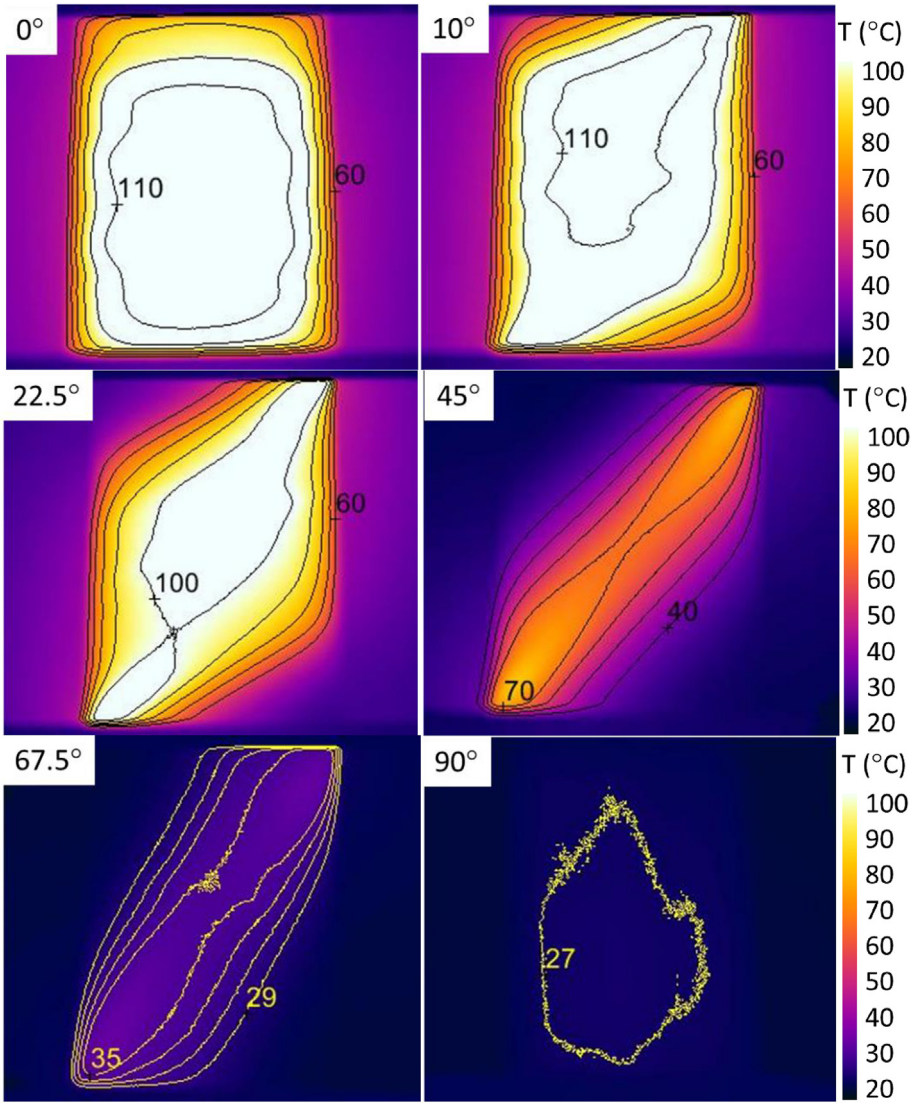

Fig. 4. Steady-state heat distribution (IR images) of the CNT web composites samples of 40 mm × 55 mm size, with different CNT web orientations at a constant 12 volts.

An infrared camera was used to observe the thermal response (Figs. 4 and 5). The current mainly flows along the CNT web alignment so most heat was generated in this orientation as illustrated by the temperature contours.

The contours of the samples in Fig. 4 are similar to the eddy current distribution of the carbon fibre-epoxy composite proposed by S. B. Pratap and W. F. Weldon [36]. At θ = 0°, heat is distributed uniformly over the whole area of the sample between the copper buses except for edge effects due to finite sample size. (Fluctuations in the 110 °C contour are ascribed to slight asymmetries in the sample preparation and testing regime). At higher angles, θ, the conductivity, and hence maximum temperature, decreases and the maximum zone shrinks to the 45° diagonal. At θ = 67.5° and higher, the area of maximum heat increases and becomes orthogonal again as the transverse conduction becomes the dominant or, at 90°, only route.

Compared with the 40 mm × 55 mm samples, 40 mm × 10 mm samples have lower electrical conductivity (except for θ = 0° or 90°) due to the higher proportion of transverse conduction at the higher aspect ratio. From 10° to 22.5° and further to 45°, the conductivity decreases sharply (Fig. 3, L/W = 4.0), consistent with the maximum temperature reached (Fig. 5). In addition, the smallest area of maximum heating is reached at 22.5° (Fig. 5) as transverse conduction dominates, rather than 45° (Fig. 4).

3.2. Effect of CNT web layup

3.2.1. Effect on electrical conductivity

In order to further improve the tuneability of the electro-thermal heating system, webs with different layup sequences were prepared (Table 2). All samples comprised four sets or units of five web layers to give 20 web layers in total. The theoretical model built in section 3.1 and the rule of mixture were combined to predict the theoretical value of specimens with different layups (Table 3). For the laminate cases with n layers of CNT web orientated at different angles, θ_i, the conductivity will be the sum of the contribution of these orientations, also under two conditions, L/W→0, Equation (5), and L/W→∞, Equation (6),

$$\sigma_{c0} = \sum_{i=1}^{n} p_{\theta_i}(\sigma_l \cos^2\theta_i + \sigma_t sin^2\theta_i) \tag{5}$$

$$\sigma_{c\infty} = \sum_{i=1}^{n} p_{\theta_i}\left[(\sigma_l \cos^2\theta_i + \sigma_t sin^2\theta_i) - \frac{(\sigma_l - \sigma_t)^2 \sin^2\theta_i \cos^2\theta_i}{\sigma_l \sin^2\theta_i + \sigma_t \cos^2\theta_i}\right] \tag{6}$$

Where $p_{\theta_i} = n_i / \sum_{i=1}^{n} n_i$ is the proportion of each orientation, or

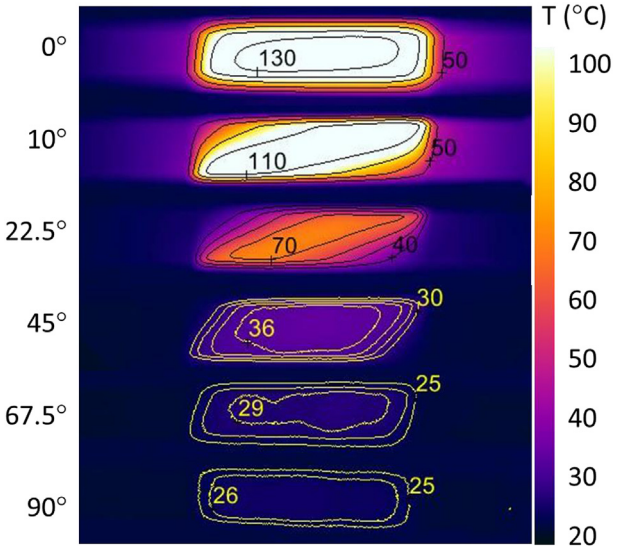

Fig. 5. Steady-state heat distribution (IR images) of the CNT web composites, at the 40 mm × 10 mm size, with different CNT web orientations at a constant voltage of 16 V.

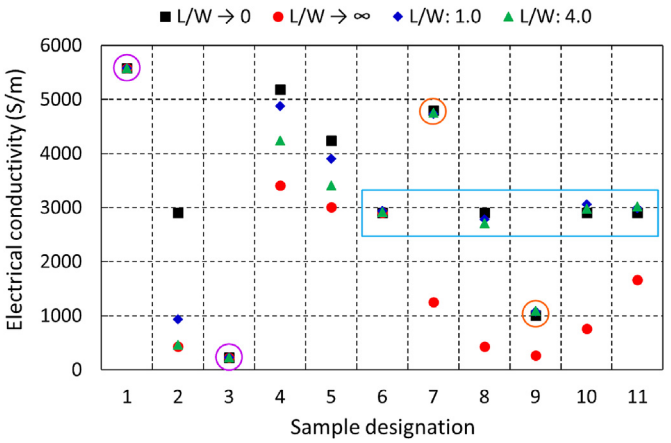

Fig. 6. Electrical conductivity of the CNT web composites at each layup pattern with two aspect ratios, L/W = 1.0 and L/W = 4.0, compared with the conductivity calculated for L/W→0 and L/W→∞.

'packing fraction' [38].

With reference to Table 3 and Fig. 6, and as in Section 3.1, sample 1 (i.e. $[0_4]$) and sample 3 ($[90_4]$) provided the lateral (σ_l) and transverse (σ_t) conductivity values respectively (circled in purple in Fig. 6). Equations (5) and (6) were used to calculate the conductivities for the L/W→0 and L/W→∞ samples with the layup shown (Table 3). Specimens with L/W of 1.0 and 4.0 were prepared and the experimental conductivities compared with calculated values (Table 3, Fig. 6).

Laminates with layup of $[0_2/90_2]$, $[+45_2/\text{-}45_2]$, $[22.5_2/\text{-}67.5_2]$, [0/+45/-45/90] (i.e. sample 6, 8, 10 and 11) with L/W of either 1.0 or 4.0 (boxed in Fig. 6), all have the same calculated value of σ_{c0} and measured values that differ ($\Delta\sigma$, Equation (7)) by less than 7%,

$$\Delta\sigma = \frac{|\sigma_e - \sigma_c|}{\sigma_c} \times 100\% \tag{7}$$

This demonstrates that when $|\theta - \varphi| = \pi/2$ and $n_1 = n_2$ ($= n_3 = n_4$ *for sample* 11), i.e. when there is an orthogonal structure, the conductivity is affected only slightly, if at all, by the position of electrodes and thus exhibits quasi-isotropic properties. As a consequence, sample 6, 8, 10 and 11 are equivalent and equation (5) reduces to,

$$\sigma^c_{\theta,\theta-\pi/2} = (\sigma_l + \sigma_t)/2 \tag{8}$$

Similarly, despite their having a fourfold difference, the electrical conductivities of samples 7 and 9 (i.e. $[+22.5_2/\text{-}22.5_2]$ and $[+67.5_2/\text{-}67.5_2]$) are also barely affected by sample geometry (circled in orange in Fig. 6) with measured values differing from σ_{c0}, by less than 8%. This can be attributed to their (in-plane) unbiased structures with respect to the applied field (Table 3). As the measurement errors of the two fundamental experimental values, σ_l and σ_t, are approximately 5%, this indicates that the conductivity of samples with various layup can be accurately predicted through this analytical model.

Interestingly, the average σ value of samples 7 and 9 equals the value of samples with a balanced orthogonal structure, i.e. sample 6, 8, 10 and 11 which satisfy equation (8). This result indicates that the electrical conductivity of laminates with unbiased layup may be merged

Table 3
Comparison of the calculated (L/W→0, σ_{c0} and L/W→∞, $\sigma_{c\infty}$) and experimental (L/W = 1.0, σ_{e1} and 4.0, σ_{e4}) results for the electrical conductivity of specimens with various CNT web layup.

Sample No.	Layup	Scheme	σ_{c0} S m^{-1}	$\sigma_{c\infty}$ S m^{-1}	σ_{e1} S m^{-1}	σ_{e4} S m^{-1} (%SD[a])
1	$[0_4]$		–	–	5578 (5.3)	
2	$[45_4]$		2902	435	938	467 (5.2)
3	$[90_4]$		–	–	226 (4.3)	
4	$[0_2/22.5_2]$		5186	3414	4878	4237 (2.8)
5	$[0_2/45_2]$		4240	3006	3903	3411 (1.3)
6	$[0_2/90_2]$		2902	2902	2933	2921 (3.0)
7	$[+22.5_2/\text{-}22.5_2]$		4794	1250	4732	4759 (2.3)
8	$[+45_2/\text{-}45_2]$		2902	435	2784	2710 (0.4)
9	$[+67.5_2/\text{-}67.5_2]$		1010	264	1078	1089 (0.4)
10	$[22.5_2/\text{-}67.5_2]$		2902	757	3060	2978 (0.2)
11	[0/+45/-45/90]		2902	1669	2984	3017 (2.9)

[a] Note: SD represents the standard deviation.

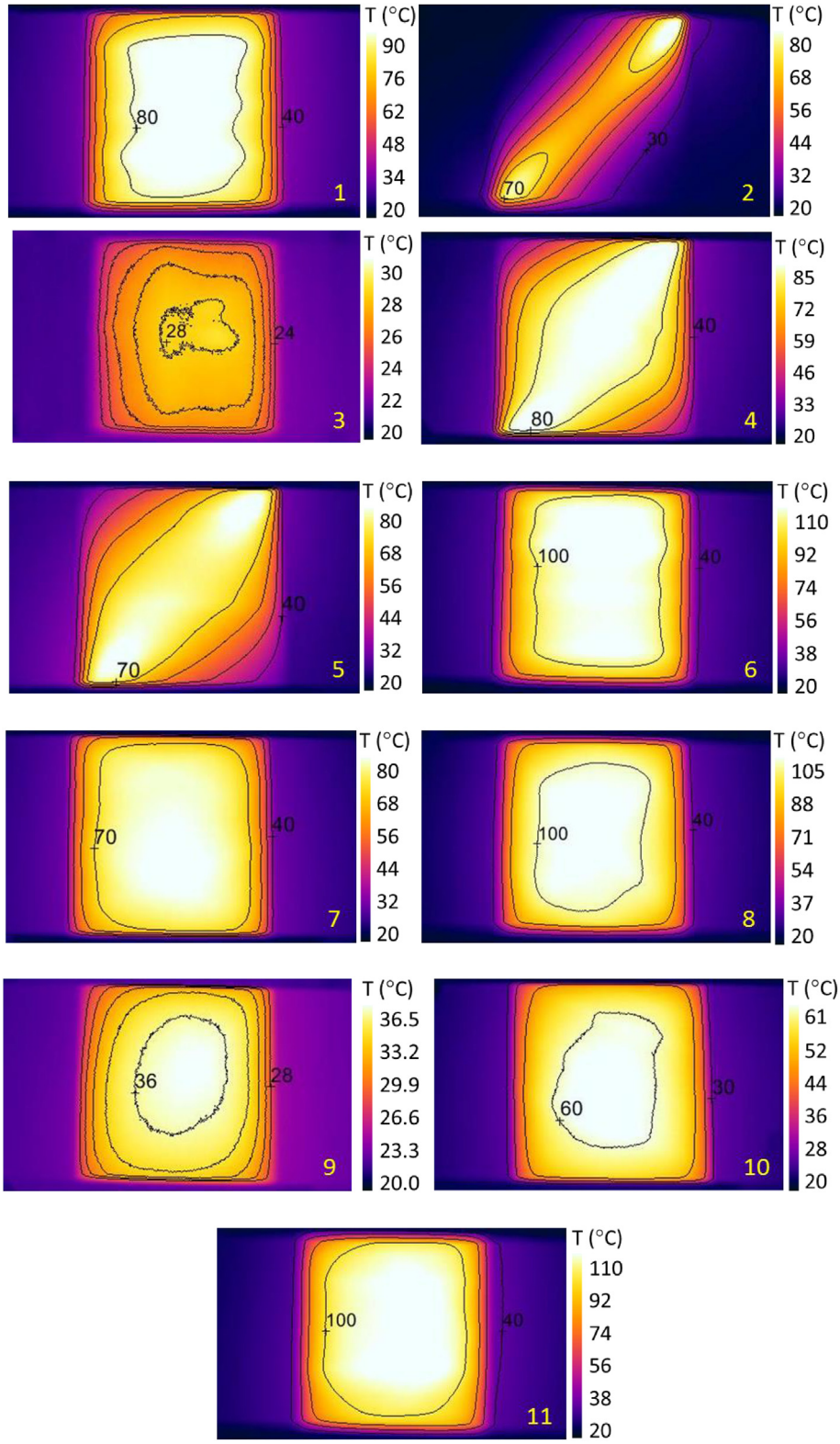

Fig. 7. Steady-state heat distribution (IR images) of the 40 mm × 40 mm specimens with various layup of CNT webs, at a constant 10 V (samples 1,4,5,7,9,10) or 16 V (samples 2,3,6,8,11) (refer to Table 3).

and separated with predictable conductivity outcomes.

For samples 2, 4 and 5 (i.e. $[45_4]$, $[0_2/22.5_2]$ and $[0_2/45_2]$), where the layup direction is strongly or completely biased compared to the field direction, sample geometry has a significant effect on their conductivity as also observed for the unidirectional samples at angles from 10° to 67.5° (section 3.1). At the lower aspect ratio, the σ_{e1} values tend toward σ_{c0}; while for the higher aspect ratio, the σ_{e4} values tend toward $\sigma_{c\infty}$. This verifies that the analytical model is also valid for predicting or at least bounding the conductivity of the samples with biased layups.

3.2.2. *Effect on heating performance*

To test the thermal performance of the CNT web with diverse

layups, samples 1, 4, 5, 7, 9 and 10 were heated by supplying a constant 10 V, and samples 2, 3, 6, 8 and 11 were heated using 16 V (Fig. 7). These voltages were chosen to yield an appropriate level of heating from the respective samples. The (in-plane) unbiased layup samples show an orthogonal temperature distribution over the region between the copper buses. The cross-ply layups (Fig. 7, samples 6,8,10,11) are slightly more regular than the unidirectional sample (Fig. 7, sample 1) as slight variations in the web uniformity would tend to be evened out, with sample [0/+45/-45/90] (Fig. 7, sample 11) perhaps being the most uniform.

The thermal performance of the biased CNT web layups (Fig. 7, samples 2,4,5) is compared to the (in-plane) unbiased example and shows a similarly biased temperature distribution as seen for the single orientation samples (Fig. 4). However, the presence of 0° in combination with the cross-oriented plies broadens the zone of maximum temperature (Fig. 7, samples 4,5) compared with a single ply orientation (e.g. at 45° Fig. 7, sample 2) and provides a degree of fine control over the location and magnitude of heating.

4. Conclusions

Electro-thermal composite specimens, with different aspect ratios and CNT web orientations, were manufactured and an analytical model, based on the thermal conductivity theory of anisotropic solids, with 'infinite' and 'finite' aspect ratios, was proposed. The model was modified to reflect the directionality of the electro-thermal structure compared with a simple thermal conductivity system. The results show that depending on the aspect ratio of the specimens, the conductivity, as a function of web orientation, is bound by the two theoretical curves for aspect ratios tending towards zero and infinity. This is consistent with results obtained for thermal conductivities of carbon fibre reinforced composites and confirmed the high alignment of the CNTs within the web. Heat distribution was monitored by an infrared camera. As the current mainly flows along the CNT web direction, most heat was generated in this orientation. Heating elements with different CNT web layups were prepared and all were shown to exhibit electrical properties which could be predicted by the analytical model, either with high accuracy for unbiased structures or within well-defined limits for highly biased layups.

This study demonstrated that CNT web orientation and layup could be used to tune and pattern the electrical conductivity, as well as the heat distribution of an electro-thermal system. Combined with previously reported parameters of CNT length and number of web layers, a highly tuneable electro-thermal system can be designed for a range of applications. Furthermore, it can also be applied to non-destructive testing of composites on a similar principle as eddy currents used for CFRP composites [39].

Acknowledgements

The authors would like to acknowledge the financial support received from the European Union's 7th Framework Programme for Research under the Marie Curie Career Integration Grant agreement No. 630756.

References

[1] V.P. McConnell, Past is prologue for composite repair, Reinf. Plast. 55 (2011) 17–21.
[2] B.G. Falzon, P. Robinson, S. Frenz, B. Gilbert, Development and evaluation of a novel integrated anti-icing/de-icing technology for carbon fibre composite aerostructures using an electro-conductive textile, Compos. Part A Appl. S. 68 (2015) 323–335.
[3] M. Mohseni, A. Amirfazli, A novel electro-thermal anti-icing system for fiber-reinforced polymer composite airfoils, Cold Reg. Sci. Technol. 87 (2013) 47–58.
[4] J. Sloan, 787 Integrates New Composite Wing Deicing System, Composites World (2008).
[5] X. Yao, S.C. Hawkins, B.G. Falzon, An advanced anti-icing/de-icing system utilizing highly aligned carbon nanotube webs, Carbon 136 (2018) 130–138.
[6] H. Chu, Z. Zhang, Y. Liu, J. Leng, Self-heating fiber reinforced polymer composite using meso/macropore carbon nanotube paper and its application in deicing, Carbon 66 (2014) 154–163.
[7] J.J. Bae, S.C. Lim, G.H. Han, Y.W. Jo, D.L. Doung, E.S. Kim, S.J. Chae, T.Q. Huy, N. Van Luan, Y.H. Lee, Heat dissipation of transparent graphene defoggers, Adv. Funct. Mater. 22 (2012) 4819–4826.
[8] V. Volman, Y. Zhu, A.R.O. Raji, B. Genorio, W. Lu, C. Xiang, C. Kittrell, J.M. Tour, Radio-frequency-transparent, electrically conductive graphene nanoribbon thin films as deicing heating layers, ACS Appl. Mater. Interfaces 6 (2014) 298–304.
[9] E.N.K. Glover, C.R. Bowen, N. Gathercole, O. Pountney, M. Ball, C. Spacie, K. Seunarine, J.M. Tour, Graphene based skins on thermally responsive composites for deicing applications, Proc. SPIE 10165 (2017) 101650G–4.
[10] D. Kim, H.C. Lee, J.Y. Woo, C.S. Han, Thermal behavior of transparent film heaters made of single-walled carbon nanotubes, J. Phys. Chem. C 114 (2010) 5817–5821.
[11] T.J. Kang, T. Kim, S.M. Seo, Y.J. Park, Y.H. Kim, Thickness-dependent thermal resistance of a transparent glass heater with a single-walled carbon nanotube coating, Carbon 49 (2011) 1087–1093.
[12] Y.H. Yoon, J.W. Song, D. Kim, J. Kim, J.K. Park, S.K. Oh, C.S. Han, Transparent film heater using single-walled carbon nanotubes, Adv. Mater. 19 (2007) 4284–4287.
[13] J. Kang, H. Kim, K.S. Kim, S.K. Lee, S. Bae, J.H. Ahn, Y.J. Kim, J.B. Choi, B.H. Hong, High-performance graphene-based transparent flexible heaters, Nano Lett. 11 (2011) 5154–5158.
[14] D. Sui, Y. Huang, L. Huang, J. Liang, Y. Ma, Y. Chen, Flexible and transparent electrothermal film heaters based on graphene materials, Small 7 (2011) 3186–3192.
[15] T.R. Pozegic, I. Hamerton, J.V. Anguita, W. Tang, P. Ballocchi, P. Jenkins, S.R.P. Silva, Low temperature growth of carbon nanotubes on carbon fibre to create a highly networked fuzzy fibre reinforced composite with superior electrical conductivity, Carbon 74 (2014) 319–328.
[16] M.K. Hassanzadeh-Aghdam, M.J. Mahmoodi, R. Ansari, Micromechanics-based characterization of mechanical properties of fuzzy fiber-reinforced composites containing carbon nanotubes, Mech. Mater. 118 (2018) 31–43.
[17] D. Janas, K.K. Koziol, Heating using carbon nanotube-based heater elements, US Patent 0366005 (2015).
[18] Y. Li, I.A. Kinloch, A.H. Windle, Direct spinning of carbon nanotube fibers from chemical vapor deposition synthesis, Science 304 (2004) 276–278.
[19] D. Janas, K.K. Koziol, Rapid electrothermal response of high-temperature carbon nanotube film heaters, Carbon 59 (2013) 457–463.
[20] X. Yao, B.G. Falzon, S.C. Hawkins, S. Tsantzalis, Aligned carbon nanotube webs embedded in a composite laminate: a route towards a highly tuneable electro-thermal system, Carbon 129 (2018) 486–494.
[21] J. Lee, I.Y. Stein, S.S. Kessler, B.L. Wardle, Aligned carbon nanotube film enables thermally induced state transformations in layered polymeric materials, ACS Appl. Mater. Interfaces 7 (2015) 8900–8905.
[22] C.J. Brampton, S.G. Pickering, C.R. Bowen, A.H. Kim, S.T. Buschhorn, J. Lee, B.L. Wardle, Actuation of bistable laminates by conductive polymer nanocomposites for use in thermal-mechanical aerosurface, 55th AIAA/ASME/ASCE/AHS/ASC Struct. Struct. Dyn. Mater. Conf., January 13-17 2014, National Harbor, Maryland, 2014.
[23] S.T. Buschhorn, N. Lachman, J. Gavin, B.L. Wardle, Electrothermal icing protection of aerosurfaces using conductive polymer nanocomposites, 54th AIAA/ASME/ASCE/AHS/ASC Struct, Struct. Dyn. Mater. Conf. Boston, Massachusetts, 2013.
[24] C. Feng, L. Jiang, Micromechanics modeling of the electrical conductivity of carbon nanotube (CNT)–polymer nanocomposites, Compos. Part A Appl. S. 47 (2013) 143–149.
[25] A.M. Marconnet, N. Yamamoto, M.A. Panzer, B.L. Wardle, K.E. Goodson, Thermal conduction in aligned carbon nanotube polymer nanocomposites with high packing density, ACS Nano 5 (2011) 4818–4825.
[26] C.P. Huynh, S.C. Hawkins, T.R. Gengenbach, W. Humphries, M. Glenn, G.P. Simon, Evolution of directly-spinnable carbon nanotube catalyst structure by recycling analysis, Carbon 62 (2013) 204–212.
[27] H.S. Jang, S.K. Jeon, S.H. Nahm, The manufacture of a transparent film heater by spinning multi-walled carbon nanotubes, Carbon 49 (2011) 111–116.
[28] D. Jung, D. Kim, K.H. Lee, L.J. Overzet, G.S. Lee, Transparent film heaters using multi-walled carbon nanotube sheets, Sens. Actuators A Phys. 199 (2013) 176–180.
[29] H. Im, E.Y. Jang, A. Choi, W.J. Kim, T.J. Kang, Y.W. Park, Y.H. Kim, Enhancement of heating performance of carbon nanotube sheet with granular metal, ACS Appl. Mater. Interfaces 4 (2012) 2338–2342.
[30] C. Feng, K. Liu, J.S. Wu, L. Liu, J.S. Cheng, Y. Zhang, Y. Sun, Q. Li, S. Fan, K. Jiang, Flexible, stretchable, transparent conducting films made from superaligned carbon nanotubes, Adv. Funct. Mater. 20 (2010) 885–891.
[31] P. Liu, L. Liu, K. Jiang, S. Fan, Carbon-nanotube-film microheater on a polyethylene terephthalate substrate and its application in thermochromic displays, Small 7 (2011) 732–736.
[32] K.R. Atkinson, S.C. Hawkins, C. Huynh, C. Skourtis, J. Dai, M. Zhang, S. Fang, A.A. Zakhidov, S.B. Lee, A.E. Aliev, C.D. Williams, R.H. Baughman, Multifunctional carbon nanotube yarns and transparent sheets: fabrication, properties, and applications, Phys. B Condens. Matter 394 (2007) 339–343.
[33] M. Musameh, M.R. Notivoli, M. Hickey, I.L. Kyratzis, Y. Gao, C. Huynh, S.C. Hawkins, Carbon nanotube webs: a novel material for sensor applications, Adv. Mater. 23 (2011) 906–910.
[34] H.S. Carslaw, J.C. Jaeger, Conduction of Heat in Solids, second ed., Clarendon Press, Oxford, 1959.
[35] D.P.H. Hasselman, H. Bhatt, K.Y. Donaldson, J.R. Thomas, Effect of fiber orientation and sample geometry on the effective thermal conductivity of a uniaxial carbon

fiber-reinforced glass matrix composite, J. Compos. Mater. 26 (1992) 2278–2288.
[36] S.B. Pratap, W.F. Weldon, Eddy currents in anisotropic composites applied to pulsed machinery, IEEE Trans. Magn. 32 (1996) 437–444.
[37] M. Weber, M.R. Kamal, Estimation of the volume resistivity of electrically conductive composites, Polym. Compos. 18 (1997) 711–725.
[38] M. Pilling, B. Yates, M. Black, P. Tattersall, The thermal conductivity of carbon fibre-reinforced composites, J. Mater. Sci. 10 (1979) 246–246.
[39] G. Mook, R. Lange, O. Koeser, Non-destructive characterisation of carbon- fibre-reinforced plastics by means of eddy-currents, Compos. Sci. Technol. 61 (2001) 865–873.